

A SIMULATION ENVIRONMENT FOR UNDULATORY LOCOMOTION[†]

Michael Sfakiotakis and Dimitris P. Tsakiris

Institute of Computer Science – FORTH
Vassilika Vouton, P.O. Box 1385, GR-71110 Heraklion, Greece
{sfakios, tsakiris}@ics.forth.gr

Abstract

This paper presents a block-based simulation environment, developed on top of Matlab/SimulinkTM to facilitate research into various aspects of undulatory robotic locomotion in biology and robotics, including assessing the effect of different body configurations on gait generation. Simulations of snake-like mechanisms are made in this environment by connecting customisable body segment blocks via appropriate joint blocks, which are activated (either by explicit joint control blocks, or by neuromuscular control blocks) to propagate a travelling wave along the mechanism. Several force models are used to characterise the interaction with the locomotion environment, and emulate crawling, walking and swimming. Simulations of anguilliform swimming are presented to illustrate the versatility of the developed tools, and the potential of their use in a variety of domains, from robotics to computational neuroethology.

Key Words: Biomechanical modelling, undulatory locomotion, Simulink

1 Introduction

The development of undulatory robotic locomotors, namely serially connected, multilink articulated robots, propelling themselves by body shape undulations, has attracted significant interest in view of existing and emerging applications related to site inspection, search-and-rescue missions, mine clearance, and even endoscopy or planetary exploration. Advantages associated with undulatory robots include terrain adaptability, modularity and redundancy, as well as their potential for use as combined locomotors and end-effectors. Most of the existing such robots utilise passive wheels to realise serpentine locomotion, via the coupling of internal shape changes to nonholonomic constraints (see [1], [2] and references therein). Snake-like robots that crawl on their underside, and do not rely on wheels (e.g. [3], [4] and [5]), as well as undulatory swimming robots (e.g. [6] and [7]) have also been developed. Inspiration is provided by biological analogues, as locomotion by transversal whole-body waves is widespread among elongated, narrow animals. It is primarily an aquatic

trait (termed *anguilliform* swimming), employed by animals ranging in size from larvae and marine annelids to sea snakes and eels. In the terrestrial environment, undulatory locomotion is utilised by snakes and lizards, and is also common among amphibians (e.g. salamanders, axolotls).

In this context, a simulation environment based on Matlab/SimulinkTM [8] has been developed, in order to facilitate research into various aspects of undulatory robotic locomotion, including assessing the effect of different body configurations, modelling the interaction with the environment, and applying neuromorphic control schemes. At the core of this development has been the SimMechanics physical modelling toolbox, used to create libraries containing elementary “body segment” blocks, which are serially connected to simulate the mechanics of planar articulated robots. The simulation environment, being versatile, expandable and relatively straightforward to work with, could have additional uses in computational neuroethology [9], or as a predictive tool in biological studies of undulatory locomotion [10].

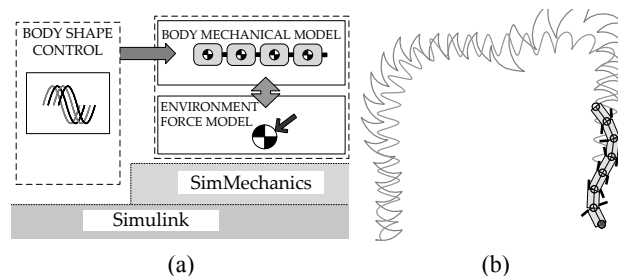


Figure 1. (a) Main components of the simulation environment. (b) Still frame from an animation, created with the results of a simulation of polychaete annelid locomotion.

2 The Simulation Environment

The simulation environment has been created on top of the Simulink substrate, to take advantage of its modular, block-based architecture, for building and integrating the main components involved in simulating an undulatory locomotor. These components are: (i) the body mechanical model, (ii) the body shape control model, and (iii) the force model of the body’s interaction with the environment (Fig. 1a).

Development is within Simulink’s graphical interface, using simple and intuitive drag-and-drop operations on the undulatory component blocks to construct the desired con-

[†]This research was supported in part by the European Commission through the IST project BIOLOCH (IST-2001-34181).

An example of such an application is provided in this section. Simulations capturing the key aspects of anguilliform swimming are set up, using the developed simulation environment, and are presented here. An undulatory mechanism, comprising $N = 7$ identical links, each with a mass m uniformly distributed across its length l , was simulated using body blocks from the developed libraries (Fig. 3).

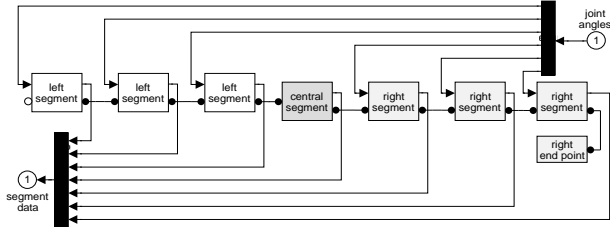


Figure 3. Mechanical model of the undulatory mechanism, constructed by serially connecting seven body segment blocks.

3.1 Fluid Drag Model

The interaction of the undulatory mechanism with the aquatic environment is simulated through a fluid drag model, which involves the following assumptions: (i) the Reynolds number is high enough for inertial forces to dominate over viscous effects (roughly for $400 < Re < 4 \cdot 10^5$), (ii) the fluid is stationary, so that the force of the fluid on a single link is due only to the motion of that link, and (iii) the pressure differentials (responsible for generating the drag forces resisting the link's motion) are considered independently for the tangential and normal directions. Then, the two components of the force applied to the i th link are respectively obtained as

$$\begin{aligned} F_T^i &= -\lambda_T \operatorname{sgn}(v_T^i) \cdot (v_T^i)^2 \\ \text{and } F_N^i &= -\lambda_N \operatorname{sgn}(v_N^i) \cdot (v_N^i)^2 \end{aligned} \quad (1)$$

where v_T^i and v_N^i are the tangential and normal components of the i th link velocity. The drag coefficients associated with each force component are denoted as λ_T and λ_N . Their value can be estimated as

$$\lambda = \frac{1}{2} \rho C S \quad (2)$$

where S is the effective area of the link, ρ is the fluid density and C is a shape coefficient. The notion of decoupled forces in the normal and tangential direction of link motion can be traced to Taylor's resistive analysis of elongated animal swimming [11], and is considerably simpler to calculate and integrate with the body dynamics than any model which requires solving the Navier-Stokes equations. It has therefore been used quite extensively in the literature (e.g. [7], [12] and [9]), despite ignoring secondary effects of water movement. Since the assumptions of this model restrict its scope to the inviscid swimming of elongated

animals, it cannot be applied to the undulatory swimming of microorganisms (e.g. nematodes and flagella), nor to the more sophisticated fish swimming modes [13].

The ratio λ_N/λ_T of the drag coefficients in Eqs. (1) is a key parameter in undulatory locomotion. The elongated body of anguilliform swimming animals (eels, amphibious snakes, etc.) is smooth and of elliptical cross-section, so that $\lambda_T \ll \lambda_N$ (Lighthill [14] estimates $\lambda_N/\lambda_T \simeq 10$ for a swimming grass-snake). Forward propulsion is then achieved by body waves propagating from head to tail [11]. Conversely, smooth elongated animals can swim backwards by reversing the propulsive wave [15]. If the animal body is not smooth, the propulsive component of the tangential force may be greater than that of the normal force (corresponding to $\lambda_N/\lambda_T < 1$). Forward motion would then be achieved by a tail-to-head wave [11]. This is indeed the case for the locomotion of errant polychaete (marine worms), whose body affords a significant amount of roughness, mainly due to the laterally projecting appendages (parapodia) distributed along their body [16].

3.2 Shape Control of the Body

3.2.1 Explicit Joint Angle Control

The most straightforward way to explicitly generate a travelling wave in a serial chain of N links is by having the joint angles vary sinusoidally, with a common frequency f and a constant phase lag ϕ_{lag} between consecutive joints:

$$\phi_i(t) = A_i \sin(2\pi f t + i\phi_{lag}) - \psi, \quad i = 1, \dots, (N-1) \quad (3)$$

where A_i is the maximum angular deflection for the i th joint (usually $A_i = A$ is assumed). The angular offset ψ provides a means for steering along curved paths, and is set to $\psi = 0$ for locomotion in a straight line. Propagation direction for the wave depends on the sign of the phase lag parameter, and is from link- N to link-1 for $\phi_{lag} > 0$. The condition $\phi_{lag} = \pm 2\pi/N$ yields (exactly) one wavelength of the propulsive wave across the undulating body, with beneficial effects on the propulsive efficiency. For links of identical length, the formulation of Eq. (3) produces a sinusoidal body shape, shown in Fig. 4 for the seven-link mechanism. The propagation velocity of the wave is calculated as $V = fw$, where w is the resulting wavelength.

3.2.2 Neural Control

A biologically-motivated body shape control method is based on central pattern generators (CPGs), which are neuronal circuits able to produce rhythmic motor patterns in an organism (for swimming, flying, breathing, etc.), even in the absence of sensory input or input from higher cognitive elements. Their behavior depends both on the intrinsic properties of the neurons that form the network, as well as on the properties of the synapses among them (connectivity, strength, etc.). Inspired by models of the CPG which

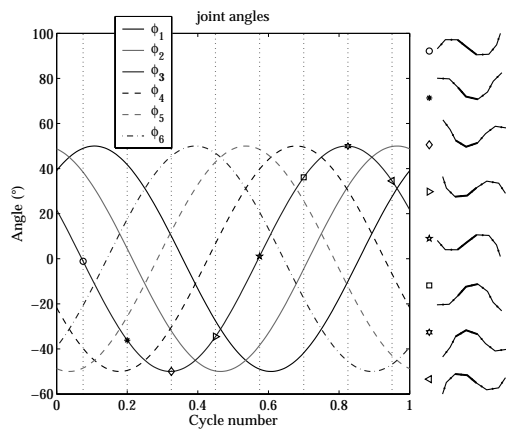


Figure 4. Relation between the joint angles and the overall body, for $N = 7$, $\phi_{lag} = 2\pi/N$, and $A = 50^\circ$. The markers follow the variation of ϕ_3 , the joint angle between links 3 and 4 (shown bold on the right).

control the undulatory swimming of the lamprey (e.g. [12], [9]), we developed Simulink blocks realising neuromuscular body shape control [5]. They are based on a connectionist CPG circuit, which is modelled as a chain of (identical) segmental oscillators, properly interconnected to generate a wave of joint activation. Each segmental oscillator is formed by two symmetrical sub-networks, which create oscillations through mutual inhibition. They comprise interneurons and motoneurons, which are all modelled as leaky integrators. The torque eventually applied to each of the body joints is determined by the outputs of the corresponding motoneurons, activating a pair of antagonistic lateral muscles, which are simulated using a spring-and-damper muscle model (Fig. 5). The characteristics of the motoneuron outputs can be altered by tonic (i.e. non-oscillating) inputs to the left and right sub-networks of the segmental oscillators.

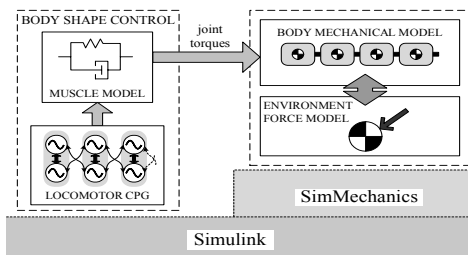


Figure 5. Neural control-based simulation scheme.

For our simulations with the basic seven-link mechanism, a body CPG, composed of 20 segmental oscillators, was constructed. The motoneuron outputs from (roughly) every third oscillator were utilised to provide torque signals to the six body joints, through the antagonistic muscles. Motion in a straight line is obtained by symmetric activation of the two sides of the body CPG, via equal tonic inputs, while turning motions are instigated by unequal tonic input to them (Fig. 6). Rapid transition in the

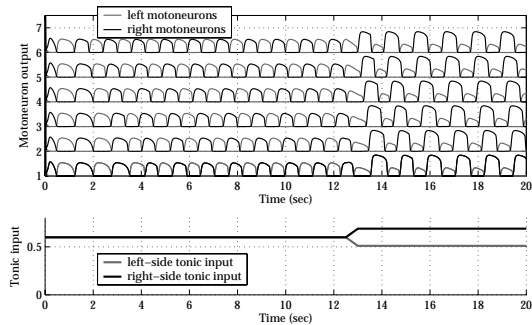


Figure 6. Tonic input and resulting motoneuron outputs of the CPG segmental oscillators, controlling the body joints.

motoneuron outputs, when varying the tonic input, is a key feature for smooth steering of the mechanism, and was found to be closely linked to the type of intersegmental coupling used in the CPG structure. The scheme was successfully applied to both smooth and rough body configurations. Since the CPG-based approach provides torque signals to the joints, their exact angular motion depends on the mechanical properties of the segments, as well as on the parameters of the force model used. The resulting joint angles are therefore quite different from the explicitly defined ones (compare Figs. 7 and 4). This fact, along with the non-straightforward interaction between the tonic input level and the properties of the motoneuron outputs (i.e. frequency and amplitude), renders the precise tuning of the travelling wave parameters difficult, and highlights the benefits of using the developed simulator for design purposes.

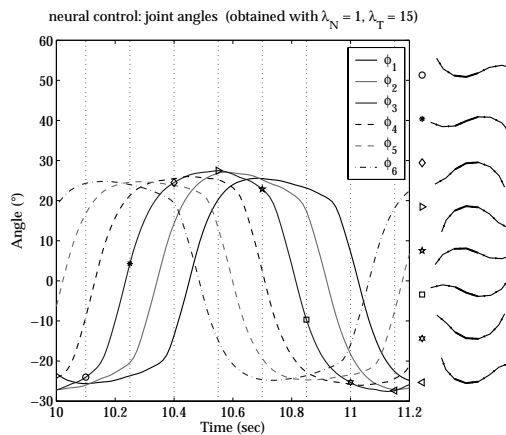


Figure 7. Joint angles and body shape, obtained using neural control to generate the travelling wave.

3.3 Simulating Qualitative Characteristics of Undulatory Swimming

This section demonstrates how the simulation environment allows the replication of the fundamental characteristics of undulatory swimming, in a series of simulations. In particular, the effect of the joint amplitude A and frequency f of the body travelling wave on swimming velocity and ef-

efficiency is assessed for different body configurations, and the main undulatory gaits are produced. The seven-link mechanism is coupled to the explicit body shape control module, using Eq. (3) to generate the propulsive wave, with $\phi_{lag} = 2\pi/N$, $A_i = A$, and $\psi = 0$. The model was run for a range of values for f (up to 4.5 Hz) and A (up to 80°), with simulations performed for both smooth (with $\lambda_T = 1$, $\lambda_N = 10$) and rough (with $\lambda_T = 10$, $\lambda_N = 1$) body configurations. Each time, the mean swimming velocity U was evaluated as the mean rate of displacement for the center of the middle link along the direction of motion, after the initial transient. Positive U values relate to motion in the opposite direction of wave propagation (eel-like locomotion), whilst for negative U values, the body moves in the same direction as the travelling wave (polychaete-like locomotion). The propeller efficiency $|U/V|$ (see [14]), was also calculated.

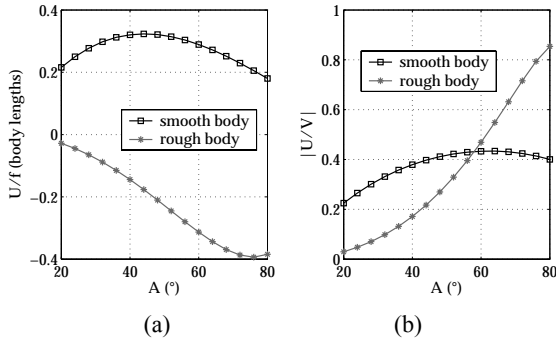


Figure 8. (a) Attained velocity and (b) propeller efficiency for the smooth and rough body configurations.

The results are compatible with Taylor's predictions [11], and correlate well with biological observations. For both body configurations, the velocity U was found to be linearly dependent on f , which is consistent with data on anguilliform-swimming animals [15], as well as with the predictions of other analytical approaches [7] and simulations [3]. This renders the U/V ratio independent of f . Results are then summarised in Fig. 8. In the smooth body case, U is moderately affected by A , with a distinct maximum appearing for $A \simeq 45^\circ$. In the rough body case, U shows a greater disparity with regard to the undulation amplitude: for values of A below $\sim 40^\circ$ the velocities achieved are very small (particularly compared to the smooth body performance with the same parameters). This is consistent with the slow swimming speed and efficiency of polychaete locomotion [16], [14]. However, as A is further increased, higher U values are attainable with this type of body configuration (at the expense of significantly increased power requirements).

In order to study the effect of the drag coefficients on U , simulations were performed for a range of λ_T and λ_N values, with $f = 1$ for $A = 35^\circ$ and $A = 70^\circ$. Simulations indicated that for both the smooth and the rough body configurations, the attained velocity only depends on the ratio of the drag coefficients, rather than on their specific values.

Results are summarised in Fig. 9.

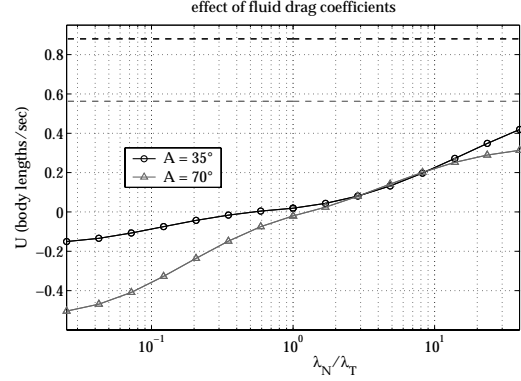


Figure 9. Attained velocities as a function of λ_N/λ_T , for two values of the joint amplitude A . Dashed lines indicate the absolute value of the respective wave velocities V .

Turning motions are obtained by introducing an offset angle $\psi \neq 0$ in the joint oscillations. Fig. 10 indicates that turning is more efficient for the smooth, than for the rough case. During turns in the smooth body case, all links follow the same mean path, while in rough body locomotion, the mean path of distal links has a distinct offset from the mean path traced by the middle link. Additional locomotion gaits (such as in-place rotation and parallel-parking) have also been implemented using variations of Eq. (3) for the evolution of the joint angles ϕ_i . In every case, the direction of motion, both translational and rotational, is determined by the λ_N/λ_T ratio.

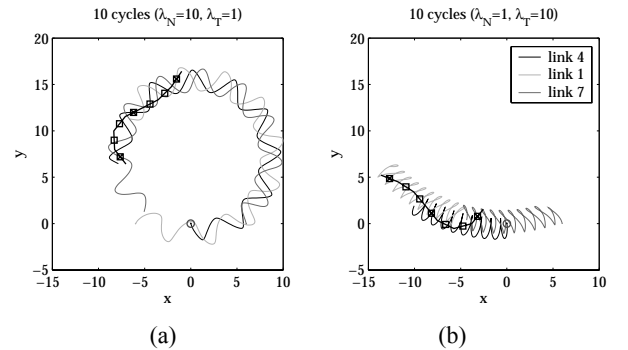


Figure 10. Link trajectories during turning motions, for (a) eel-like and (b) polychaete-like configurations. Parameters were set as $A_i = 30^\circ$, $\phi_{lag} = 51.4^\circ$, $\psi = 12^\circ$, and $f = 1$.

3.4 Replicating Biological Data

This section demonstrates how the simulation environment allows the replication of biological data for organisms locomoting by undulations, thus becoming a useful tool both for the analysis of such data, and for designing new biological experiments.

Simulations were set up based on the detailed biological data from filmed sequences of swimming of the *Anguilla anguilla* eel, which are provided in [15]. A biomechanical eel model has been constructed (total body length

$L = 22$ cm, and total mass $M = 13$ g), comprising 20 links, of equal length and cylindrical in shape, to reflect the analysis framework in [15], and incorporating the biometric measurements reported therein. The Reynolds number for the reported eel swimming kinematics is around $Re \approx 3 \cdot 10^4$, thus validating the use of the fluid drag model in the simulations; the drag coefficients were calculated using Eq. (2) and set to $\lambda_N = 0.5$ kg/m and $\lambda_T = 0.01$ kg/m. The explicit joint angle control scheme is used to generate the travelling wave in the developed eel model.

Two simulation runs are presented here, corresponding to two of the representative eel swimming sequences analysed in [15] (one for forward, and one for backward propulsion). From the pool of biological data for the two selected sequences, the reported frequencies and maximal angles between segments, along with the body contour plots, were used to set the parameters f , A_i and ϕ_{lag} in Eq. (3). Results were then evaluated by comparing the attained velocities and body amplitude profiles obtained in simulation, against the corresponding measurements in [15]. For both the forward and the backwards sequences, a very good match has been obtained (Fig. 11). We have also been able to reproduce a number of additional observations (regarding, for example, the orientation changes of the head), made in [15], on the eel swimming kinematics, and their relation to body shape and mass distribution.

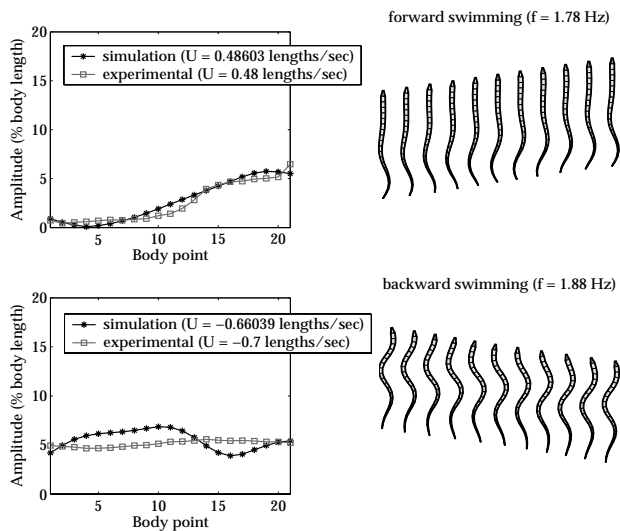


Figure 11. Amplitude profiles (left) and body contour plots (right) for simulations of forward and backward eel swimming. Body points refer to the endpoints of the eel sections considered in [15].

4 Conclusions

The simulation environment described above could facilitate the study of undulatory locomotion principles, both in biological organisms and in related robotic implementations. Further extensions will include the expansion to three-dimensional mechanisms and motions (which is made possible by the built-in support of SimMechanics for 3D models), the incorporation of additional models for the

interaction of the undulatory mechanism with its environment, and the enhancement of the neural control modules with sensory feedback (both proprioceptive and exteroceptive), which will modulate the CPG network.

References

- [1] S. Hirose, *Biologically Inspired Robots: Snake-Like Locomotors and Manipulators*. New York: Oxford University Press, 1993.
- [2] P. Krishnaprasad and D. Tsakiris, "Oscillations, SE(2)-snakes and motion control: A study of the roller racer," *Dynamical Systems*, vol. 16, no. 4, pp. 347–397, 2001.
- [3] M. Saito, M. Fukaya, and T. Iwasaki, "Modelling, analysis, and synthesis of serpentine locomotion with a multilink robotic snake," *IEEE Control Systems Magazine*, vol. 22, no. 1, pp. 64–81, 2002.
- [4] S. Ma, W. Li, and Y. Wang, "A simulator to analyze creeping locomotion of a snake-like robots," in *IEEE Conference on Robotics and Automation (ICRA'01)*, pp. 3656–3661, 2001.
- [5] D. Tsakiris, A. Menciassi, M. Sfakiotakis, G. La Spina, and P. Dario, "Undulatory locomotion of polychaete annelids: mechanics, neural control and robotic prototypes." The Annual Computational Neuroscience Meeting, Baltimore, July 2004 (to appear).
- [6] J. Ayers, C. Wilbur, and C. Olcott, "Lamprey robots," in *Proc. of the International Symposium on Aqua Biomechanisms* (T. Wu and N. Kato, eds.), 2000.
- [7] K. McIsaac and J. Ostrowski, "A geometric approach to anguilliform locomotion: Modeling of an underwater eel robot," in *IEEE Conf. on Robotics and Automation (ICRA'99)*, pp. 2843–3848, 1999.
- [8] The MathWorks Inc., *Using Simulink - version 5*. 2003.
- [9] A. Ijspeert, "A connectionist central pattern generator for the aquatic and terrestrial gaits of a simulated salamander," *Biological Cybernetics*, vol. 85, no. 5, pp. 331–348, 2001.
- [10] B. Webb, "Robots in invertebrate neuroscience," *Nature*, vol. 417, pp. 359–363, May 2002.
- [11] G. Taylor, "Analysis of the swimming of long and narrow animals," *Proceedings of the Royal Society (A)*, vol. 214, pp. 158–183, 1952.
- [12] Ö. Ekeberg and S. Grillner, "Simulations of neuromuscular control in lamprey swimming," *Phil. Trans. of the Royal Society of London Series B*, vol. 354, no. 1385, pp. 895–902, 1999.
- [13] M. Sfakiotakis, D. Lane, and J. Davies, "Review of fish swimming modes for aquatic locomotion," *IEEE Journal of Oceanic Engineering*, vol. 24, no. 2, pp. 237–252, 1999.
- [14] J. Lighthill, "Hydromechanics of aquatic animal propulsion - a survey," in *Mathematical Biofluidynamics*, pp. 11–44, Bristol: J.W. Arrowsmith Ltd., 1975.
- [15] K. D'Aout and P. Aerts, "A kinematic comparison of forward and backward swimming in the eel *Anguilla anguilla*," *Journal of Experimental Biology*, vol. 202, no. 11, pp. 1511–1521, 1999.
- [16] R. Clark and D. Tritton, "Swimming mechanisms in nereidiform polychaetes," *Journal of Zoology*, vol. 161, pp. 257–271, 1970.